



Thermomechanical characterisation of a thermoplastic polymer and its short glass fibre reinforced composite: Influence of fibre, fibre orientation, strain rates and temperatures

Peihao Song^{a,b}, David J. Chapman^{a,b}, Aaron M. Graham^{a,b}, Bratislav Lukić^c, Alexander Rack^c, Clive R. Siviour^{a,*}

^a Department of Engineering Science, University of Oxford, Parks Road, OX1 3PJ, UK

^b DPI, P.O. Box 902, 5600 AE Eindhoven, the Netherlands

^c ESRF The European Synchrotron, CS 40220, F-38043 Grenoble Cedex 9, France

ARTICLE INFO

Keywords:

Fibre reinforced polycarbonate
High strain rate
Adiabatic heating
High rate in-situ characterisation

ABSTRACT

Polycarbonate composites are widely used in products exposed to high strain rate deformation. This paper investigates the thermomechanical properties of polycarbonate and 20 wt% glass fibre reinforced polycarbonate to provide characterisation data and improved mechanistic understanding of the response to load, supported by Dynamic Mechanical Analysis and time-temperature superposition. Compressive behaviour is characterised from 0.001 to 5000 s⁻¹ at room temperature and from -60 to 120 °C at 0.01 s⁻¹; and a thermal imaging camera used to obtain temperature rise data. Quasi-static tensile experiments were also performed in different orientations relative to the injection flow direction. High-rate compression experiments are performed with X-ray imaging. As well as information about rate dependence of yield stresses and softening in the two materials, these data show how adiabatic shear band formation can cause significant softening in the composite. These data will enhance application of these polymers and facilitate development of advanced thermo-mechanical models.

1. Introduction

Polycarbonate (PC) is a widely used glassy thermoplastic polymer with good mechanical, thermal, and electrical properties [1]. However, the pure polymer does not have high enough strength and stiffness for some structural applications [2]. Adding short fibres into thermoplastics is a common way to significantly improve their mechanical response [3]. Short fibre reinforced composites (SFRCs) are becoming increasingly popular owing to fast, inexpensive manufacturing compared to laminated composites [3]. This fast-growing demand for SFRC leads to a requirement for reliable material characterisation methods and data to understand and model mechanical behaviour [4].

The mechanical properties of SFRCs are highly dependent on fibre content, fibre orientation, interfacial adhesion strength, and polymer matrix properties [3,4]; typical fibre lengths are of order 0.2 to 0.4 mm [4,5]. Anisotropic stiffness and strength are an unavoidable result of SFRC manufacture, e.g. through injection flow-induced fibre orientation, and mechanical properties can also vary between different parts of a manufactured product because of changes in flow conditions [6,7].

Furthermore, manufacturing history, e.g. processing temperature and cooling rate, can result in variations in the thermomechanical responses of the matrix polymer [8,9].

Polycarbonate composite components used in automotive, aeronautics, and sports engineering applications are likely to be exposed to mechanical loading at various strain rates and temperatures. It is well known that the temperature-dependent mechanical properties of polymer materials are attributed to their molecular transitions, such as the secondary (β)- and glass (α)-transitions, and, for PC, the temperatures of these two transitions are about -50 and 145 °C [10]. Some aspects of the subsequent response under quasi-static loading conditions have been characterised, such as the effect of fibre flow orientation [11,12] or fibre weight fraction [4], fatigue behaviour [6], influence of fibre type and interfaces [13], impact of manufacturing process [4,14], and tribological properties [15]. However, unlike pure polycarbonate, fewer studies have investigated the time and temperature-dependent properties of short fibre reinforced PC (SFPC), particularly high strain rate behaviours.

The split Hopkinson pressure bar (SHPB) allows the characterisation

* Corresponding author.

E-mail address: clive.siviour@eng.ox.ac.uk (C.R. Siviour).

<https://doi.org/10.1016/j.compositesa.2024.108099>

Received 15 November 2023; Received in revised form 25 January 2024; Accepted 18 February 2024

Available online 20 February 2024

1359-835X/© 2024 The Authors. Published by Elsevier Ltd. This is an open access article under the CC BY license (<http://creativecommons.org/licenses/by/4.0/>).

of polymers and polymer composites in uniaxial compression at strain rates from about 10^2 to 10^4 s⁻¹ [16–21]. For polycarbonate, Siviour *et al.* [22] and Mulliken and Boyce [23] reported that the yield stress increases with strain rate, with a more significant dependence at rates above ~ 1000 s⁻¹; this observation was attributed to the secondary (β)-transition [10,22]. An equivalent effect is, of course, observed by lowering the temperature at a single strain rate, providing the chance to replicate the high rate behaviour using quasi-static low temperature data [24,25]. In recent years, the SHPB system has also been used to investigate the dynamic compression properties of thermoplastic polymer composites such as polyamide 66 composite [26], polyester composite [27] and PEEK composite [28]. Nevertheless, to our knowledge, no research has yet been published on dynamic compression response of PC-based composites.

One of the key features of large plastic deformation is the temperature rise that occurs from the conversion of plastic work to heat. At high strain rates, in which the experiment is adiabatic, this temperature rise can have a significant effect on the mechanical responses of polymeric materials [16]. These effects include but are not limited to thermal softening for polymer resins [29,30] and adiabatic shear failure for polymer composites [31]. Thus, quantifying the temperature rises under different loading conditions is essential to fully understand the constitutive behaviour. These measurements have been made for PC using Infra-Red (IR) detectors [29,32–37], IR cameras [34,38] and embedded thermocouples [33,39]. For composites, embedded thermocouples can aggravate the anisotropic behaviour and accelerate the failure process; in addition, as a point-measurement, the full-field thermal gradient information induced by strain localisation during large strain deformation would be missed. This can be important, for example, in recent studies [27,31,40], high rate compression behaviours of fibre reinforced polymer laminate were measured using an SHPB with an IR camera; all the samples showed nonuniform thermal distribution as a result of the strain localisation. Hence, even though the fastest thermal cameras can only give a small number of full-field images (say 3–5) with a useful spatial resolution, thermal imaging is the most appropriate approach to measuring temperature rises in composite materials.

In the study reported here, the rate and temperature dependent compression behaviour of PC and injection moulded 20 wt% glass fibre reinforced PC composite were characterised at rates from 0.001 to 5000 s⁻¹ at room temperature and temperatures from -60 to 120 °C at 0.01 s⁻¹. These rates were chosen to support implementation of these materials in industrial environments. Similarly, the upper temperature is likely to be the maximum operating temperature for PC components, as the material softens significantly above this temperature. The lower temperature was chosen to encompass the effect of the β -transition, and thereby provide an understanding of the interrelationship between rate and temperature; however, this is also a reasonable operating temperature in some applications (e.g. aviation). The room temperature experiments were instrumented with a thermal camera to measure temperature rise in the specimens. To support these experiments, frequency sweep DMA tests were performed to understand the time-temperature dependent viscoelastic behaviour of both materials, as well as fibre and fibre flow orientation effects. Tensile tests with different loading speeds were also performed to characterise dependence on injection direction and loading rate effects. Together, these provide a complete dataset for evaluating and developing constitutive models. To better understand the mechanics of damage formation at high strain rates, and support model development, further dynamic compression experiments were performed using an SHPB at beamline ID-19 of the European Synchrotron Radiation Facility (ESRF), with samples cut in different orientations relative to the injection moulding flow direction. These experiments aimed to explore the capability of single-bunch X-ray phase contrast imaging (XPCI) to investigate the incipient stages of internal damage formation, fibre delamination, and fibre breakage during high-rate deformation of the polycarbonate composite. Radiographs from these experiments were analysed using

digital image correlation (DIC), exploiting the microstructural heterogeneity of the composite to understand the strain distribution (localisation) during tests, this was compared to temperature rises measured using the IR camera in other experiments. Here it is noted that some of the stress-strain data from the PC matrix have been published in [10]; however, all the composite data and temperature rise data are unique to the current paper.

2. Material information and sample preparation

The polycarbonate matrix (LEXANTM 500R resin) and a composite made by combining this resin with 20 wt% short glass fibre were provided by SABIC® as $175 \times 175 \times 3$ mm sheets manufactured by injection flow moulding; the fibre length was from 0.2 to 0.4 mm, and the fibre diameter was between 0.01 and 0.02 mm. Both materials were annealed by heating at 25 °C/hour to 155 °C, which is 10 °C above the glass (α)-transition temperature, holding at this temperature for six hours and cooling at 10 °C/hour to room temperature. T_g was measured using the second heat cycle in heat-cool-reheat differential scanning calorimetry (DSC) tests [10]. The annealing process minimises residual stresses from manufacturing and ensures that the materials have the same thermal history, so that the effects of fibre can be investigated more explicitly.

Samples for all experiments were cut from the centre of the annealed sheets, as indicated in Fig. 1(a). For the composites, tensile samples were cut in three directions, 0° (injection flow direction), 45° and 90° ; the sample dimensions were chosen according to ISO 527 type 1BA, Fig. 1(b). Three-point bend DMA samples, with a length of 60 mm, width of 10 mm and thickness of 3 mm, were also cut in these three directions. For the pure PC matrix, it was assumed that there are no orientation effects and specimens were cut in one direction only. For mechanical characterisation experiments, compression samples for both materials were obtained by cutting specimens through-thickness (TT) with a 5 mm diameter and 3 mm thickness. For the in-situ X-ray experiments on the composite, two different types of compression specimens were made: all were 2×2 mm cylinders with the subsequent loading direction through-thickness or in the injection flow direction as indicated in Fig. 1(a).

3. Experimental procedures

3.1. Dynamic mechanical analysis (DMA)

Experiments were performed on a TA Instruments Q800 DMA. Previous research [10,41] has shown that the storage modulus obtained from DMA experiments in three point bend are consistent with results from tensile experiments. Therefore, in the current study experiments were conducted in three point bend on specimens with a span of 50 mm, width of 10 mm and thickness of 3 mm, consistent with ASTM standard D4065 and our previous study [10]. Careful calibration of apparatus and fixtures was conducted prior to the experiments according to the manufacturer's instructions. Isothermal frequency sweep experiments were performed at frequencies of 0.2, 0.5, 1, 2, 5 and 10 Hz, over a temperature range from -110 to 180 °C at 2 °C/min temperature increments with a five-minute isothermal equilibrium time before gathering data at each temperature.

3.2. Tensile tests

A screw-driven Instron 5980 universal test machine mounted with a 100 kN load cell was used to perform tension tests at room temperature. The samples were tested under displacement control at 10, 1 and 0.1 mm/min. Engineering stress-strain curves were calculated using force data from the load cell and the cross-head displacement.

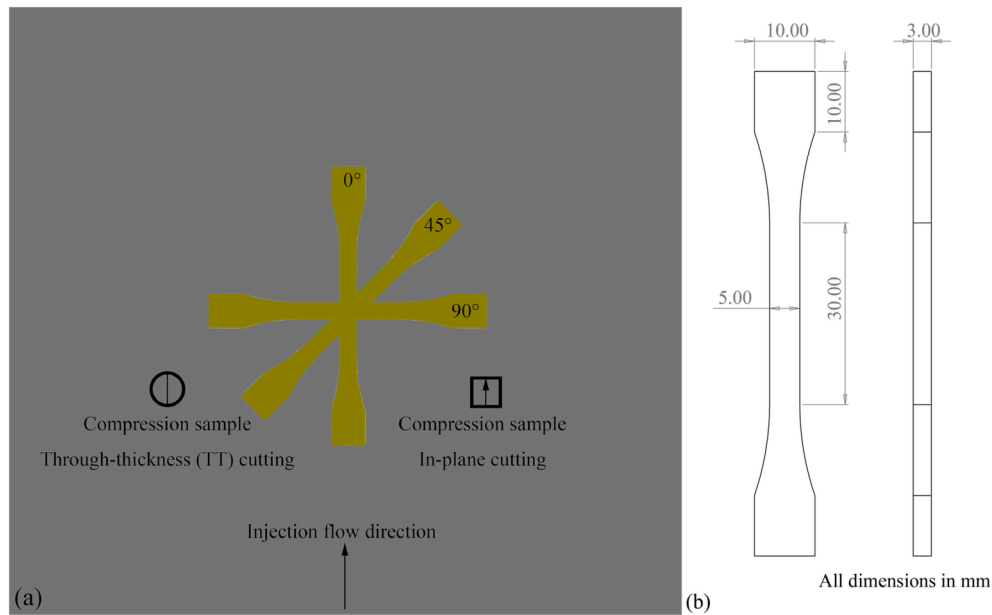


Fig. 1. (a) Schematic of sample cutting, (b) Dimensions of tension sample.

3.3. Compression experiments

The true rate controlled quasi-static (QS) experiments from 0.001 to 0.5 s^{-1} were conducted using the same test machine as the tensile tests; however, strain was measured using an extensometer mounted to the anvils close to the specimen, shown in Fig. 2(a). The temperature dependent compression experiments were performed at 0.01 s^{-1} from -60 to 120°C using the same machine with an environmental chamber. Here, a digital thermometer was attached to the load anvil to monitor the chamber temperature before and during testing. Petroleum jelly lubricant was used in room and high temperature tests, and AERO-SPEC® 210 graphited grease at low temperatures.

Medium rate measurements from 1 to 60 s^{-1} were conducted using a hydraulic machine; the displacement was measured by the averaged value obtained from a pair of linear variable differential transformers (LVDTs), and force was obtained by a strain-gauge based load cell (Fig. 2(b)). A long split-Hopkinson pressure bar (LSHPB) with a 2000 mm striker was employed for experiments from 400 to 750 s^{-1} , and SHPB from 1000 to 5000 s^{-1} , Fig. 2(c). To achieve both a high rate and large strain, an LSHPB with a shorter striker (1000 mm) was utilised to characterise the material properties at around 2500 s^{-1} . In all high-rate tests, cylindrical specimens were sandwiched between Ti-6AL-4 V input and output bars. The input reflected and output waves were measured

using gauges attached to bars. Readers are referred to the literature for a more detailed review of the SHPB system [42]. Following the suggestions in [43], a thin brass film was attached to the input bar to form a pulse shaper, as shown in Fig. 2(c), to reduce the oscillations in the input bar induced by wave dispersion. Petroleum jelly was used to lubricate the interface between bars and specimen for all medium and high rate experiments. It is worth noting that each low and medium strain rate compression test was repeated three times; representative data are shown here but all data will be made available online. Data from all high-rate experiments are shown.

3.4. Thermal measurements

A TELOPS FAST-IR M3K IR camera with a 50 mm lens and 0.75 in. extension ring was used to measure the temperature rise during deformation at room temperature. Before testing, the factory camera calibration was carefully verified using a calibrated black body source from 50 to 150°C . The transmissivity of the sapphire window (used in high rate tests) was also confirmed using the black body source over the same temperature range. Finally, the emissivity of the two PC materials was measured as 0.97 using a calibrated emissivity surface and a temperature-controlled black panel. This value is very close to the value from 0.92 to 0.96 in the literature [44]. The temperature error

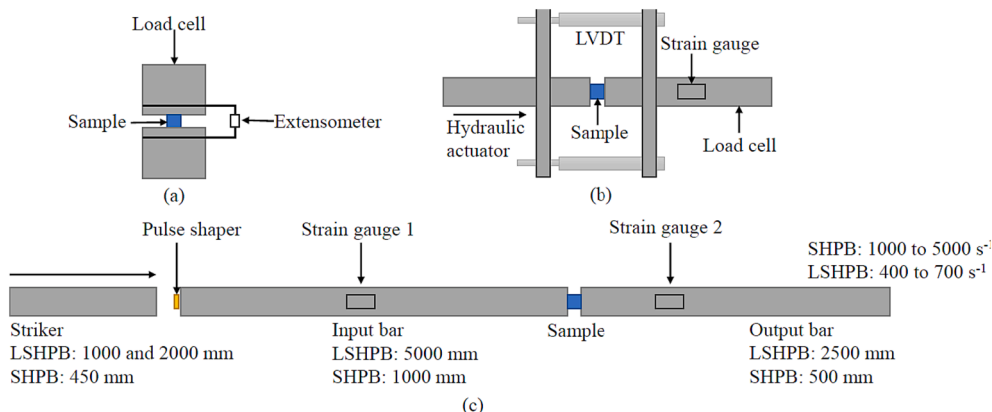


Fig. 2. (a) Screw-driven tests, (b) Hydraulic machine, (c) Split Hopkinson pressure bar.

introduced by changing the calibration in this range is approximately 1.5 °C for a measurement of 130 °C and consequently, all data were reduced using a constant mid-range emissivity of 0.95. For QS and medium rate tests, a complete sequence of images can be taken using this IR camera, rates of 100 and 500 frames per second were used. However, the speed of the IR camera was insufficient to adequately resolve the thermal evolution during the high-rate Hopkinson bar tests. Here, the IR camera was used with a 10 000 Hz frame rate and 20 μ s exposure time, and was triggered when the striker impacted the input bar. A monitor signal from the camera was recorded alongside the strain gauge signals to allow alignment of the IR images and the strain gauge data (appropriately time-shifted). In this case, a single experiment of 400 to 500 μ s duration can provide four or five images. In order to increase the utility of images from different experiments, the trigger delay of the camera was then altered in 20 μ s steps. In this way, and having checked that the data between experiments are consistent, a series of images can be constructed by stitching a number of single tests together. Table 1 gives further details about the IR camera settings for all sets of experiments.

3.5. In-situ X-ray experiments

In-situ dynamic measurements on PC composites were performed at the ID-19 beamline at the European Synchrotron Radiation Facility (ESRF) [45]. The SHPB system includes a 1300 mm input bar, an 1100 mm output bar and a 400 mm striker with 12.7 mm diameter, and all components were aluminium alloy (7075 T6); more detailed information, such as schematics of an experimental setup can be found in [46], and details of synchronisation and similar imaging system in [31,47,48]. The cylindrical composite samples were sandwiched between 1 mm thick aluminium anvils to protect the end of the aluminium bars. This study used the 16-bunch filling mode (75 mA storage current), with the X-ray pulse width of ~ 60 ps measured in [49], separated in time by ~ 176 ns, and the white beam from the two axially aligned U32 undulators, filtered with 3.2 mm of diamond, and 0.7 mm of aluminium to reduce the heat load of the sample and the imaging system. The white beam was gated during the experiment using a fast-shutter which remained open for approximately 15 ms. These experiments aimed to visualise the internal failure process and deformation localisation occurring during the high-rate compression of the filled polycarbonate specimens. Consequently, these experiments employed a 10 \times magnification coupled to an indirect X-ray detector assembly, providing an approximately 1.28 \times 0.8 mm field of view and a pixel size of 3.2 μ m. To improve the signal to noise ratio in the resulting radiographs, 16 Be-based compound refractive lenses were used to compress the X-ray beam into the magnified field of view. In order to enhance the visualisation of the fibres and the presence of cracks, the imaging system was located within the near-field diffraction regime, facilitating edge enhancement by propagation based X-ray phase contrast [47,50]. The X-ray beam having transmitted through the specimen, and propagated over approximately 1.2 m, was converted to visible light by a LYSO:Ce single crystal (150 μ m thickness), and captured by a Shimadzu HPV-X2 camera, employing a 200 ns exposure time and 880 ns interframe time. Consequently, radiographs were formed from every fifth X-ray bunch (with minimal ghosting) in the 16 bunch filling mode, recording 128 frames over a total duration of nearly 120 μ s. The strong image contrast produced by the edge enhancement of the XPCI technique was exploited

to perform DIC analysis to track the deformation of the specimen.

4. Experimental results

4.1. DMA results

DMA data for the PC matrix materials and specimens of the composite cut in three orientations are shown in Fig. 3(a). In all tests, the modulus shows the effect of the secondary (β)-transition below -40 °C, followed by a slowly decreasing modulus with increasing temperature. A very rapid decrease is observed at about 130 °C, but the three point bend configuration does not allow measurements above this temperature because of the low specimen stiffness. All the filled materials have a higher modulus than the PC matrix; as expected, this depends on the specimen orientation. Time-temperature superposition (TTS) was used to construct master curves, Fig. 3(b), to estimate the rate dependent storage modulus and aid later interpretation of the compressive data. Fig. 3(c) plots the relationship between the TTS shift factor and temperature; the PC matrix shows the most considerable variation from low to high temperature, followed by 90° and 45° samples. The temperature sensitivity of the 0° PC composite is lower than the other specimens, consistent with this behaviour being dominated by the temperature insensitive fibres.

4.2. Tensile test results

All materials show rate-dependent behaviour, Fig. 4: an increase in loading speed increases the failure stress for PC composites and the yield stress for PC matrix. All PC specimens were tested to a final engineering strain larger than 120 %, whilst the PC composite failed at strains around 5 %. The stiffnesses derived from these data were quantitatively consistent with the DMA test results: further, a higher loading speed increases the stiffness, and specimens cut from the fibre direction are stiffer than in other directions at the same speed. It is also noted that the failure stress of the specimen cut from the transverse direction (90°) is very close to the yield stress of the pure matrix material.

4.3. Compression test results

Fig. 5(a) and 5(b) present the compressive response of the PC matrix and PC composite at a constant true strain rate of 0.01 s⁻¹ at temperatures from -60 to 120 °C. Three tests were performed at each temperature; here, one true-stress strain curve and all three yield stresses are plotted. In all these experiments, the specimen is assumed to deform at a constant volume when calculating the true stress. In this section, all PC composite specimens are made by through-thickness (TT) cut, which means the specimens were loaded perpendicular to the fibre flow orientation.

The PC matrix shows a very obvious yield, followed by softening and hardening during deformation at all temperatures, and the yield stress increases from 55 to 120 MPa with decreasing temperature. The temperature dependent yield stress of PC composite has the same trend; the yield stress increases with decreasing temperature, from 65 to 174 MPa. However, the softening was less than observed in the matrix material, and not observed at all at high temperatures, such as 90 and 120 °C. Research in the literature [51–53] has reported that the glass transition temperature (T_g) of the interface region of polymer based composite materials is much lower than the pure matrix material. This means that in these higher temperature experiments, for PC composite, part of the matrix might already be above its T_g , removing the softening process after yield, which is only seen in polymers below the glass transition.

The rate dependent compression responses are shown in Fig. 6(a) and 6(b) for the PC matrix and PC composite, respectively. The yield stress for both materials shows a bilinear increase with an increased log strain rate over seven decades, as shown in Fig. 6(c); this is caused by the secondary (β) transition [10,22].

Table 1
IR camera settings for all experiments.

Strain rate (s ⁻¹)	Frame rate (Hz)	Exposure time (μ s)	Window size (pixel ²)
0.01, 0.1, 0.5	100	100	128 \times 128
1.5 \pm 0.2, 12.5 \pm 2.5	500	100	300 \times 160
2500 \pm 200	10,000	20	128 \times 92

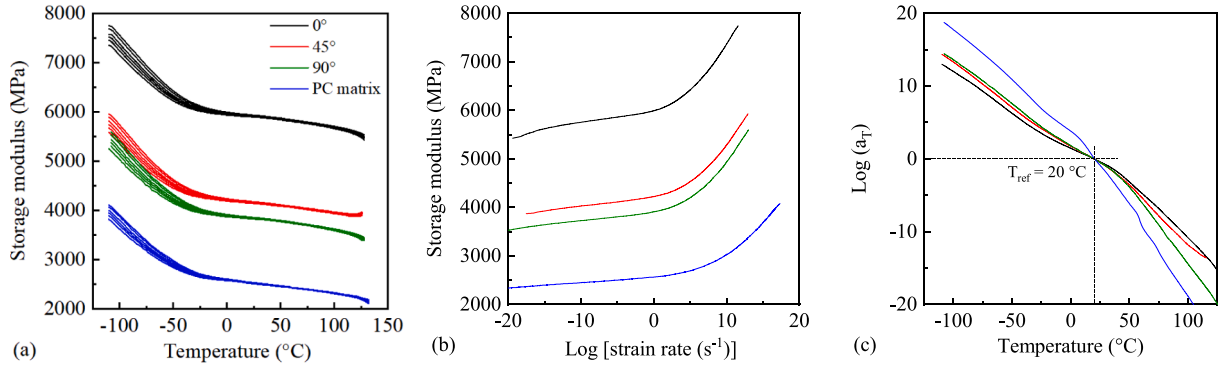


Fig. 3. (a) Storage modulus against temperature, (b) Time-temperature superposition master curves at 20 °C, (c) Shift factor versus temperature.

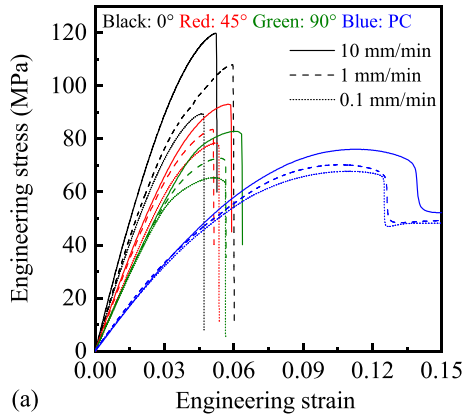


Fig. 4. Engineering stress–strain curves at three different loading rates for the composite cut in three orientations relative to the injection flow direction and PC matrix (representative specimens shown here, raw data provided online for all specimens tested).

By comparing Fig. 5(c) and Fig. 6(c), it is observed that both PC matrix and PC composite show time-temperature equivalence: decreasing temperature and increasing strain rates both increase yield stress. To explore this further, low temperature and high-rate stress-strain data are compared for both materials in Fig. 7. These agree well for strains lower than 0.3. Above this strain, for the PC matrix, more softening is found at rates of 1 and 60 s⁻¹ relative to the ‘equivalent’ QS experiment at low temperatures, but this is not observed in high rate tests (i.e. 530 and 3100 s⁻¹), for which the stress-strain curves are almost identical. For the PC composite, obvious softening can be seen, relative to the ‘equivalent’ low temperature results, in both medium (12 and 40 s⁻¹) and high rate (4300 s⁻¹) experiments. All rate dependent

experiments in Fig. 7 experience adiabatic heating of the specimen; thus, to further understand the observed behaviour, temperature rise data are presented in the next section.

4.3.1. Temperature rise measurements for PC matrix

Temperature rise measurements were performed in QS (0.01, 0.1 and 0.5 s⁻¹), medium rate (1.1 and 11 s⁻¹) and high rate (~2600 s⁻¹) experiments. Of interest is temperature rises in higher rate experiments in which heat does not have time to conduct out of the specimen on the timescale of the experiment. It is possible to estimate the strain rate above which this happens using the following equations [10,24]:

$$\alpha = \frac{k}{\rho C_p} \quad (1)$$

$$l_t = 2\sqrt{\alpha t} \rightarrow t = \frac{1}{\alpha} \left(\frac{l_t}{2} \right)^2 \quad (2)$$

$$\dot{\epsilon} = \frac{1}{t} \quad (3)$$

Here α is thermal diffusivity, k thermal conductivity (0.2 W m⁻¹ K⁻¹), ρ density (1.2 g cm⁻³), and C_p specific heat capacity (1.2 J g⁻¹ K⁻¹). The timescale (t) of thermal diffusion can be estimated using Equation (3), where, l_t is the length of the specimen. Using this 1-D approximation, the transition from isothermal to adiabatic conditions starts at a rate of around 0.06 s⁻¹ for a full length (3 mm) sample. This is consistent with experimental observations: the temperature rise at a rate of 0.01 s⁻¹ is only 2 °C (for strain = 0.8), which only has a small effect on the mechanical properties; the equivalent rise at 0.1 s⁻¹ is about 9 °C, and 20 °C at 0.5 s⁻¹.

Fig. 8 shows selected thermal images and mean temperature data from two quasi-static compression experiments. In the thermal images, the mean temperature within the white dotted box is recorded and

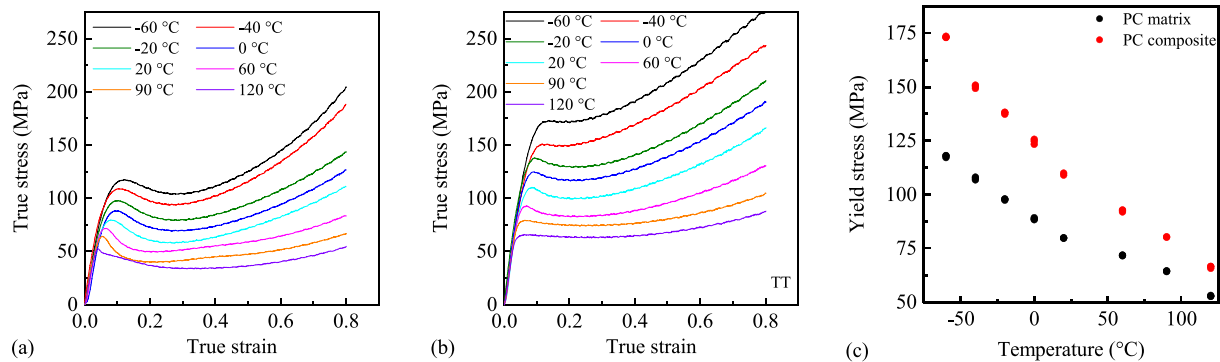


Fig. 5. (a) Temperature dependent stress–strain curves for PC matrix, (b) Temperature dependent stress–strain curves for PC composite (TT), (c) Yield stress versus temperature for PC matrix and composite.

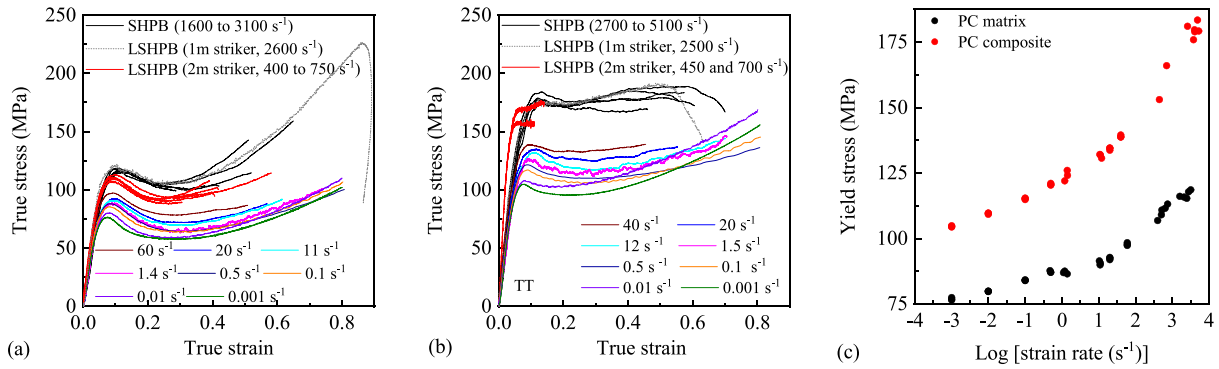


Fig. 6. (a) Rate dependent stress–strain curves for PC matrix, (b) Rate dependent stress–strain curves for PC composite (TT), (c) Yield stress versus logarithm strain rate for PC matrix and composite.

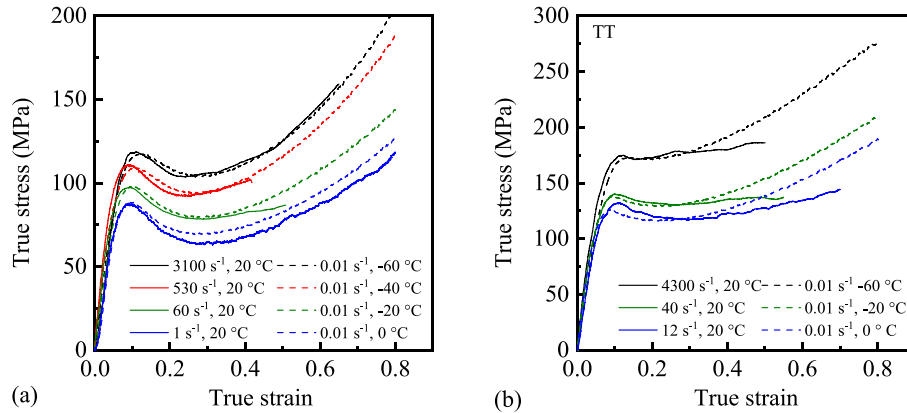


Fig. 7. Comparison of stress–strain curves at low temperatures and high strain rates; the colours indicate which temperature and rate combinations are equivalent. (a) PC matrix, (b) PC composite (TT).

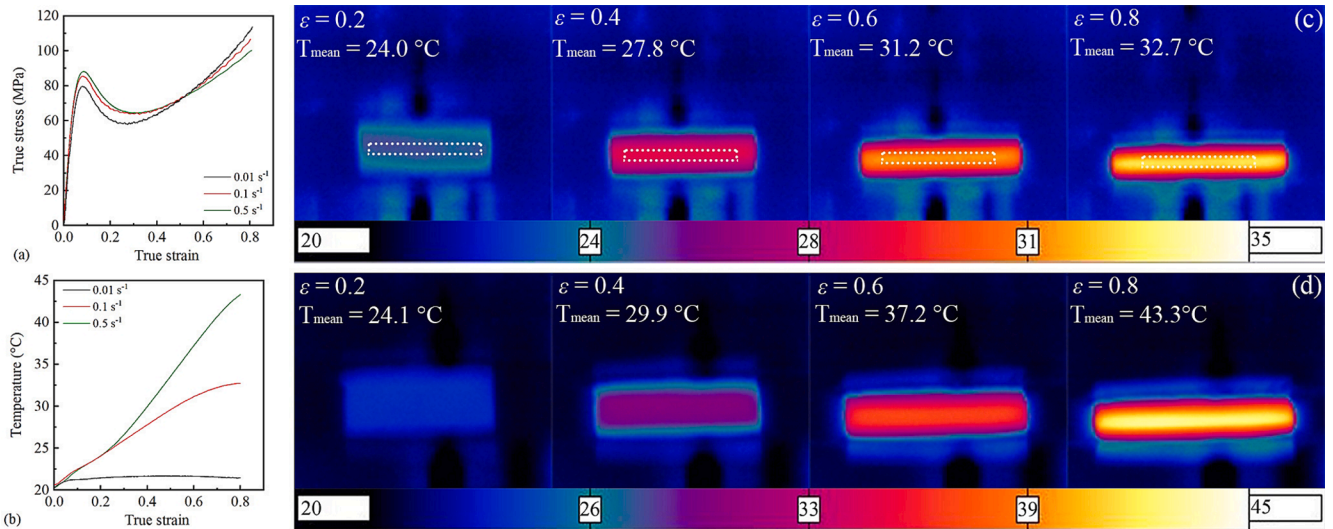


Fig. 8. (a) stress–strain data for three quasi-static experiments on PC; (b) mean temperature rise data obtained from thermal images of these experiments; (c) selected thermal images from experiment at 0.1 s⁻¹, (d) selected thermal images from experiment at 0.5 s⁻¹.

shown as T_{mean} . Here, we see the larger temperature rises at the higher strain rate of 0.5 s⁻¹, which we expect to be close to adiabatic; hence, the data obtained are consistent with increased thermal losses at the lower rate due to the increased importance of conduction.

Temperature rises were measured in medium rate experiments at 1.5 and 11 s⁻¹, Fig. 9. The strain rate control in these experiments is not as

good as in the quasi-static tests, and when interpreting these data, the departure from a constant strain rate at large strain apparent in Fig. 9(b) must be considered. The stress at 11 s⁻¹ is higher than in the lower rate test until a strain of around 0.7, after which the loading ends in the higher rate test. This is consistent with the thermal images: the higher rate tests show higher temperature rises for strains lower than 0.7, whilst

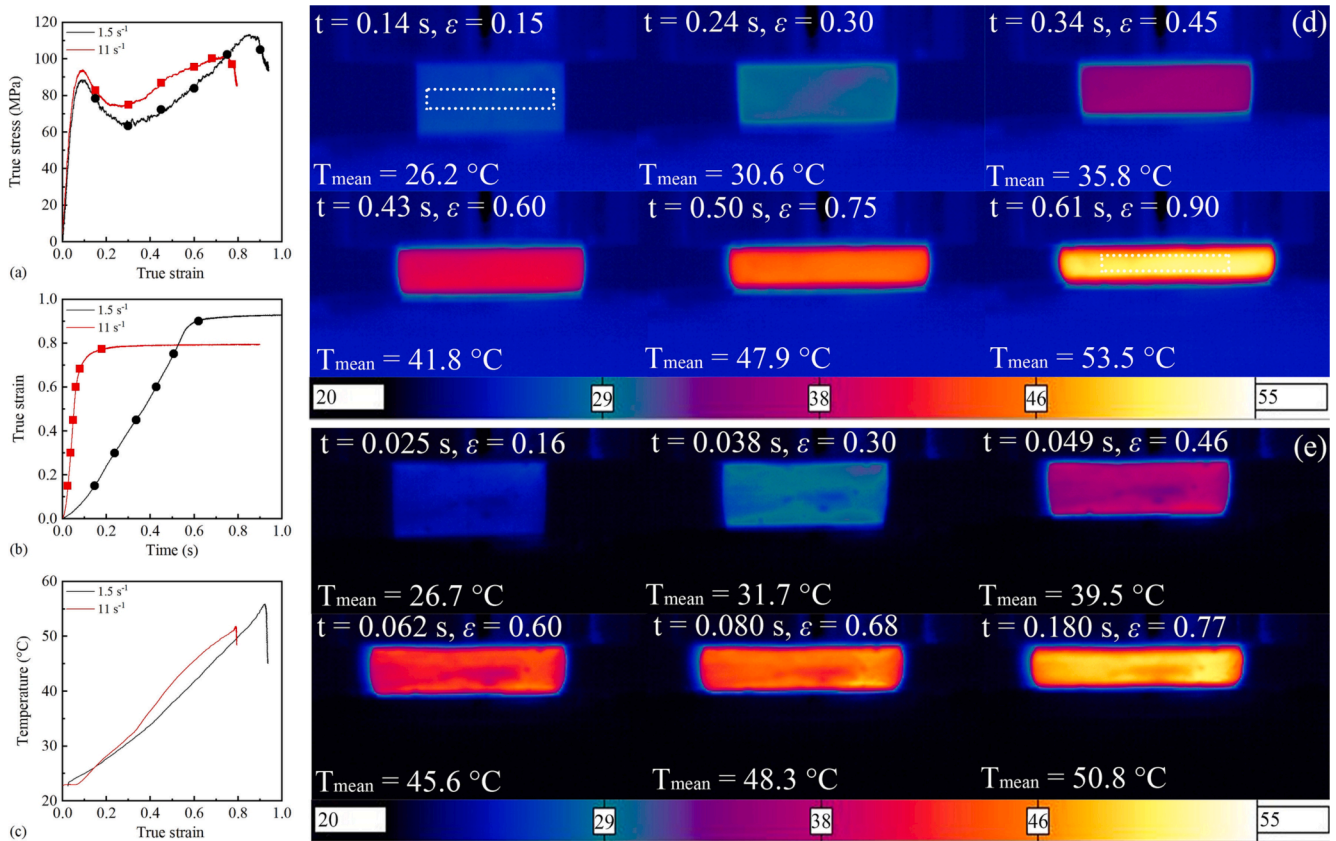


Fig. 9. (a) True stress versus true strain curves in two medium rate tests on PC; (b) true strain versus time data for the same experiments; (c) mean temperature-true strain; (d) selected thermal images from experiment at 1.5 s⁻¹, (e) selected thermal images from experiment at 11 s⁻¹. Markers on the stress-strain and strain-time curves indicate when the thermal images were taken.

the temperature for the 1.5 s⁻¹ test is higher at the end of the deformation because the strain is larger.

Eight experiments were conducted at a strain rate of 2500 ± 200 s⁻¹ using the long split Hopkinson bar and instrumented with the high speed IR camera, which can provide 3 to 5 thermal images during the loading period. The IR camera was triggered at a different time for each experiment, and as shown in Fig. 10(b), this changes the timing of the exposure relative to the stress pulse in the specimen. The mean temperatures obtained from each thermal image were then combined to form the temperature versus strain curve in Fig. 10(c). The maximum temperature is ~ 80 °C at 0.86 strain; however, as discussed above there is less softening in the stress-strain curve compared to equivalent isothermal (low rate) experiments performed at low temperature. This observation is consistent with previous work on PC [24,25,36]. Further investigations are required to understand the relationship between temperature rise and the mechanism of softening and hardening in high rate experiments for the PC matrix.

4.3.2. Temperature rise measurements for PC composite

The same methodology is used to measure the temperature rise for PC composites. According to the thermal parameters of a similar product (LEXANTM FR RESINS 3412R, 20 wt% glass fibre reinforced polycarbonate) [54], the 3 mm specimen experiences adiabatic conditions at strain rates above 0.07 s⁻¹; similarly to the pure PC specimens, with the decrease in sample length, this rate will be changed. Fig. 11 shows the temperature rises obtained in the quasi-static experiments. Here, both mean and maximum temperature rises are shown, because in later experiments at medium and high strain rates localisation is observed, leading to very high temperature rises in regions of the specimen. Here, the maximum and mean temperatures are very close to each other for both strain rates, indicating that strain localisation is not apparent in

these quasi-static tests. Similar to the matrix material, the temperature rise at 0.5 s⁻¹ is higher than at 0.1 s⁻¹, indeed the temperature in the low-rate experiment is observed to decrease at higher strains as the heat dissipates into the anvils. For the PC composite, the strain at which the stress in the 0.01 s⁻¹ exceeds 0.1 and 0.5 s⁻¹ is lower than for the PC matrix. This might be because more heat is generated in the PC composite than in the pure matrix material at the same rate (Fig. 8 and Fig. 11).

Fig. 12 presents measurements made at medium rates, 1.4 and 11.4 s⁻¹. The initial yield stress at the higher rate is larger; however, later in the experiments, the stress at 1.4 s⁻¹ exceeds that at 11.4 s⁻¹ when the strain is over 0.45. This might be caused by greater thermal softening at 11.4 s⁻¹. Unlike the experiments reported above, an uneven thermal distribution is observed in Fig. 12(c) and (d), e.g. the difference between the maximum and mean temperatures is 5.5 °C and 7.9 °C at strain around 0.3 for the compression tests at 1.4 s⁻¹ and 11.4 s⁻¹ respectively. After that, the difference between the maximum and mean temperatures decreases. The temperature patterns in these images indicate that strain localisation occurs in the medium rate experiments but is somewhat homogenised during the deformation process.

For the high rate experiments, samples (TT cut) were tested in two directions relative to the flow orientation: with the flow direction parallel to the camera and with the flow direction toward the camera, Fig. 13(a) and 13(b). In order to obtain a full sequence of images, the same stepped trigger timing over multiple experiments as described in Fig. 10(b). The strain rates are 2500 ± 200 s⁻¹, and the stress-strain curves agree well for different experiments. In fact, it was found that the maximum and mean temperature values measured in the two directions overlap very well, the orientation has no significant effects.

These temperature rise data help us to interpret the differences between high rate experiments and the 'equivalent' low temperature

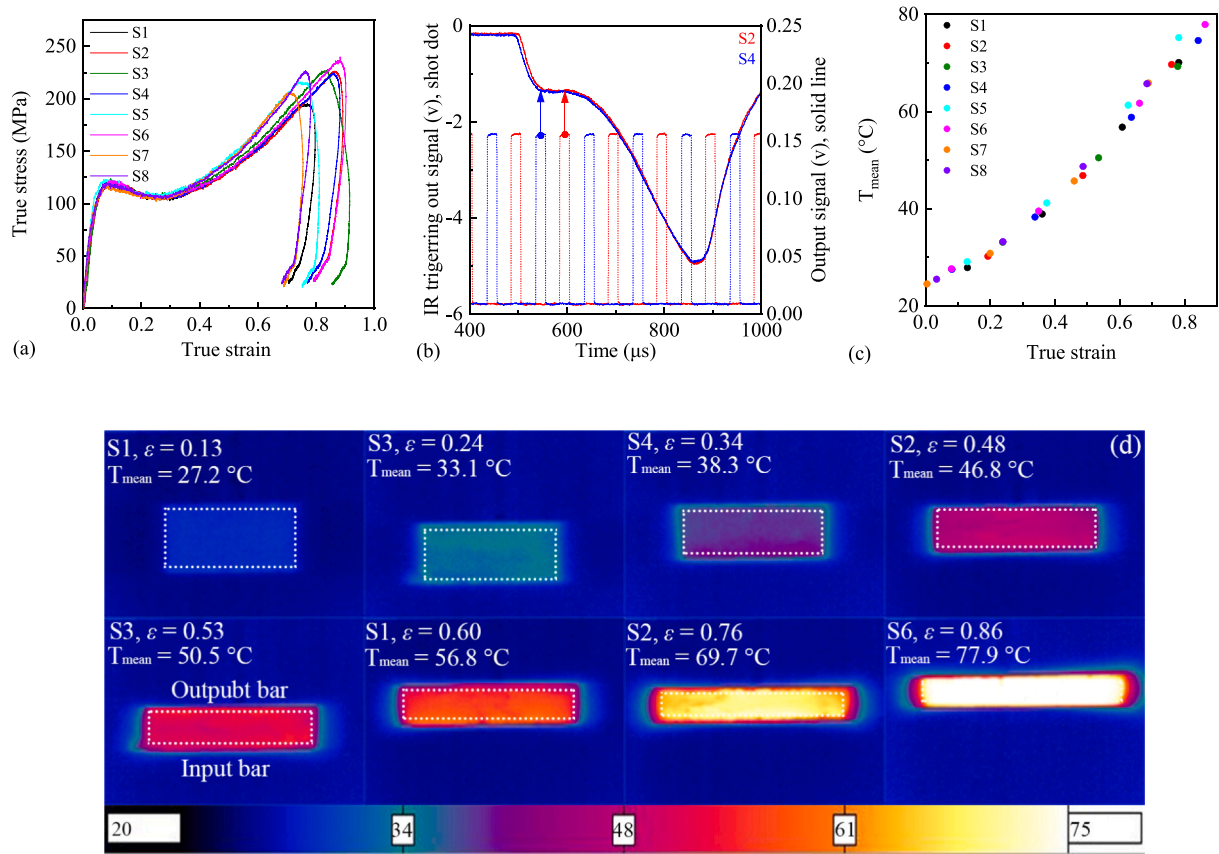


Fig. 10. (a) True stress versus true strain curves for eight Hopkinson bar experiments on PC; (b) Time-shifted IR monitor out signal and LSHPB output bar signal from two experiments; (c) Mean temperature rise versus true strain for all the images obtained, the numbers S1-S8 indicate the eight different specimens tested; (d) Selected thermal images from low to high strain, montage produced from a number of experiments, again the numbers S1-S6 indicate from which specimen the image was obtained.

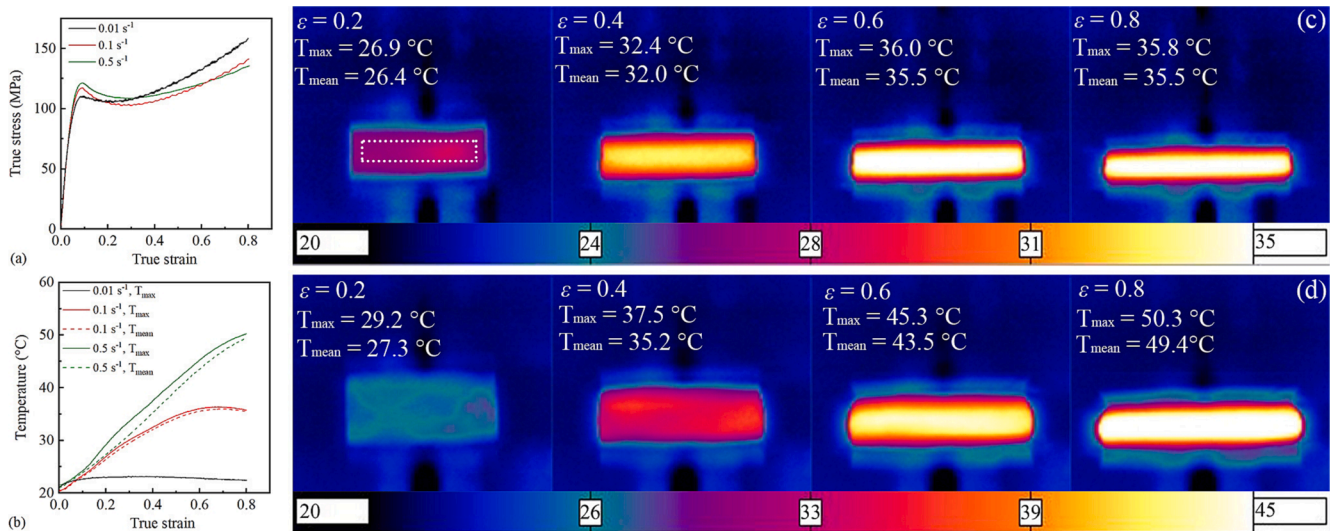


Fig. 11. (a) stress–strain data for three quasi-static experiments on PC composite; (b) maximum and mean temperature rise data obtained from thermal images of these experiments; Temperature against true strain at different rates; (c) selected thermal images from experiment 0.1 s^{-1} ; (d) selected thermal images from experiment at 0.5 s^{-1} .

quasi-static test with the same yield stress, e.g. Fig. 7(b). The stress–strain curves begin to diverge at a true strain of about 0.3, at which the maximum temperature is around $50 \text{ }^{\circ}\text{C}$, indicating that thermal softening is important in these experiments on composite materials. As the high rate experiment progresses, the local maximum temperature

approaches $80 \text{ }^{\circ}\text{C}$ at a strain of around 0.6, which may approach the T_g of the interface material as discussed above. Following this, an apparent stress drop is observed (Fig. 13(a) and 13(b)) and very large temperature rises are seen in the thermal images (Fig. 13(d) and 13(e)), indicating the formation of an adiabatic shear band. At this point, temperatures in the

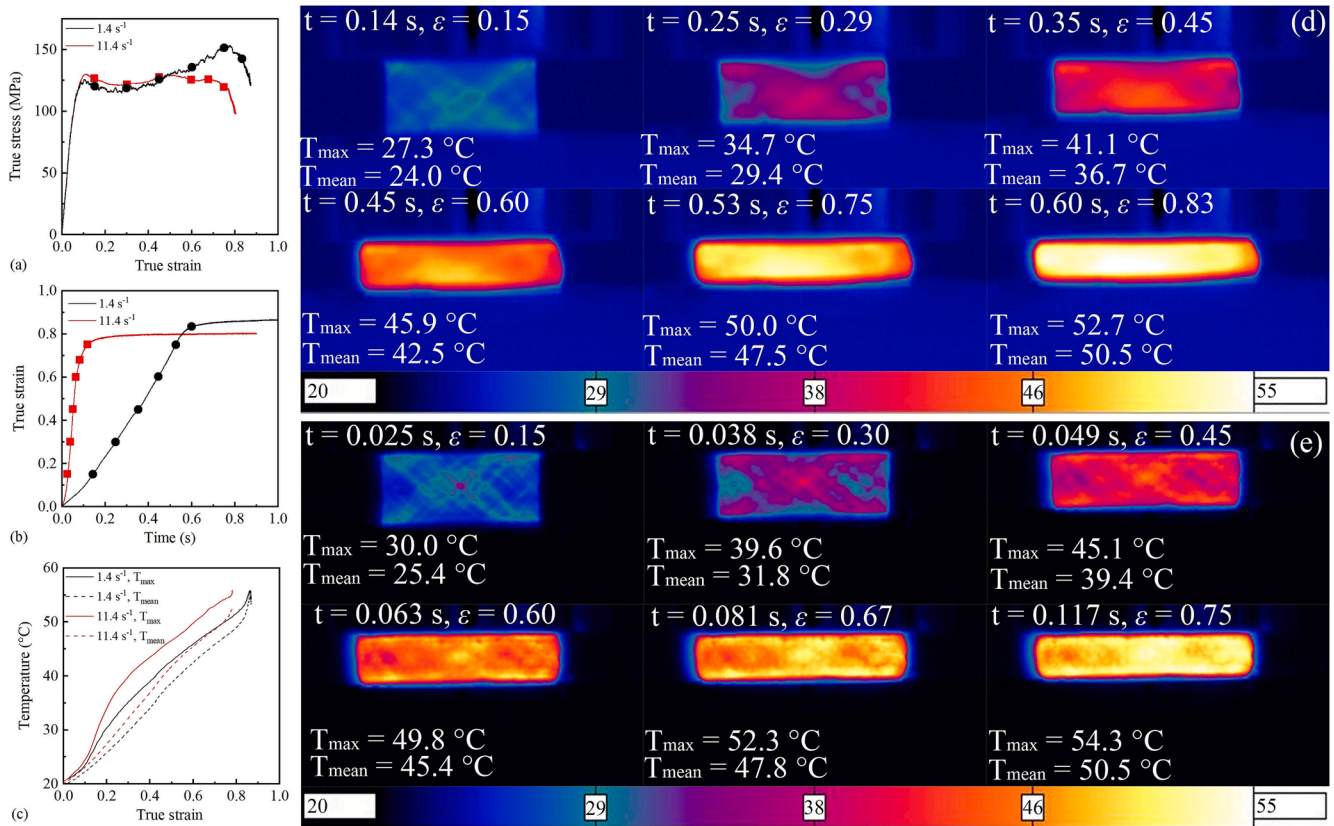


Fig. 12. (a) True stress versus true strain curves in two medium rate tests on PC composite; (b) true strain versus time data for the same experiments; (c) maximum and mean temperature vs true strain; (d) selected thermal images from experiment at 1.4 s⁻¹, (e) selected thermal images from experiment at 11.4 s⁻¹. Markers on the stress-strain and strain-time curves indicate when the thermal images were taken.

specimen exceed the softening temperature indicated by DMA (Fig. 3 (a)). This is accompanied by a rapid increase in overall strain rate as the material softens (Fig. 13(b)). The divergence between experiments at these larger strains is probably due to small differences in microstructure (e.g. fibre alignment, fibre distribution, interface behaviour) and the effect this has on the formation of the adiabatic shear bands.

The softening of high rate tests after yield but before the stress drop might be caused by localised heating in the specimen or micro-failure during the loading process, this is explored further below, whilst the significant stress drop after strain over 0.6 is due to the adiabatic shear band. It appears that in medium rate experiments localisation starts, but there is sufficient time for the higher temperature regions to lose heat to surrounding material before they become hot enough to form shear bands.

4.3.3. Dynamic in-situ measurements in ESRF

In-situ experiments were conducted in the European synchrotron radiation facility (ESRF) to examine microstructure evolution during the high rate tests. For these experiments, smaller specimens were used (2 mm long and 2 mm diameter), and these could be cut in a number of orientations: through-thickness specimens were equivalent to the specimens used in all the experiments above, although smaller, and could again be loaded with the injection flow direction parallel to the imaging plane (i.e. P) or perpendicular to the imaging plane (i.e. T). In plane specimens were loaded along the injection flow direction (see Fig. 14). Here, it is noted that the macroscopic response is the same as obtained in earlier experiments, showing that there is no significant effect from the X-rays.

Firstly, the mechanical data are compared to those obtained in the other Hopkinson bar experiments, see Fig. 14(a) and (b). Here, the yield and flow stresses are consistent for the specimens loaded through

thickness, Fig. 14(b); for the specimen loaded along the fibre flow direction, the yield stress is the same (a), but there is significant post-yield softening. X-ray images were obtained at a rate of 1.6 MHz, Fig. 15(a), (b), (c) show four images spaced through the duration of loading, no microcracking was observed in these images. In order to further explore the deformation, Fig. 15(a'), (b') and (c') show full-field strain maps produced using DIC on the X-ray images obtained at global strains (determined from the timing of the image relative to the strain history from the SHPB) of 0.07, 0.15, 0.25 and 0.35 for three 2 × 2 mm samples in different orientations; further information about the DIC processing is given in the Appendix. In performing this analysis, it is acknowledged the speckle contrast used in the DIC analysis is formed from the projection through the entire specimen rather than from a single plane within the specimen, and consequently, the resulting strain maps produced are interpreted cautiously, particularly as strain increases. To address this, a future study will seek to employ high density particles located on a known specimen plane to form the speckle contrast. Nonetheless, all strain maps indicate strain localisation, consistent with the thermal images in Fig. 13(d) and (e).

In order to link global and local behaviours of this inhomogeneous material, the temperature rise is used as a 'bridge'. We start by considering the strain dependence of the mean temperature rise in the (homogeneously deforming) PC and the local maximum temperature rise in the (inhomogeneous) PC composite, obtained from the results in the preceding sections, Fig. 16(a). Then, the local temperature rises in the composite can be inferred from the DIC strain measurements and our knowledge of the expected temperature rises in the PC matrix at those strains, assuming that the matrix sees most of the strain and, on these timescales, most of the heating. The result obtained is shown in Fig. 16 (b); here, for each X-ray image, the global strain is measured, and the expected maximum temperature is then found using a line fit to the

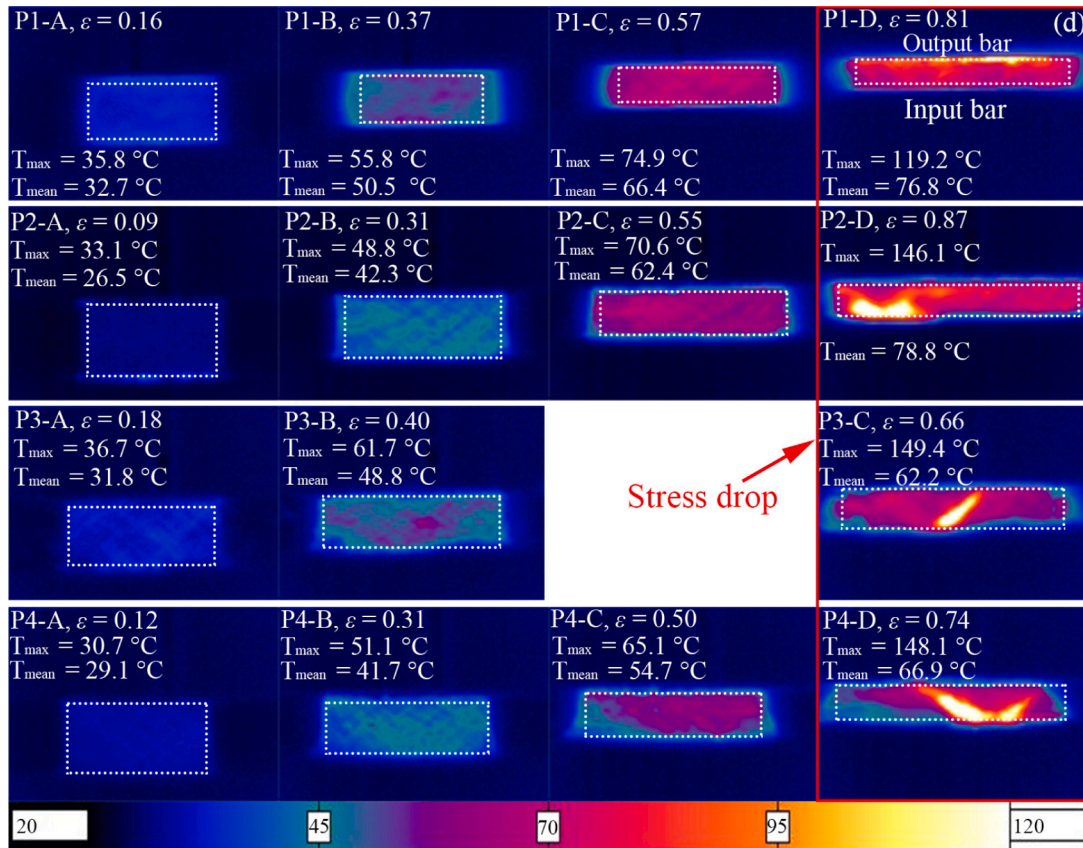
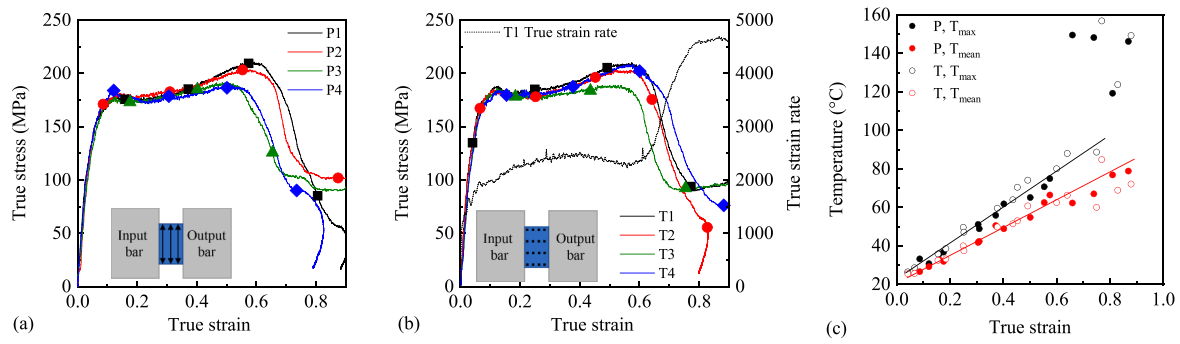


Fig. 13. Temperature rise measurements in high rate experiments on PC composite (a) True stress-true strain curves for fibre flow parallel to the IR camera (P), markers indicate when the IR images were taken; (b) True stress-true strain curves for fibre flow towards the IR camera (T), note that the stress-strain behaviour for P and T is the same, but the data are shown separately for easier comparison to the thermal images; (c) Temperature rise measurements for the eight experiments; (d) Thermal images for fibre flow parallel to the IR camera, (e) Thermal images for fibre flow towards the IR camera (note that green colour indicates that the temperature has exceeded 150 °C. (For interpretation of the references to colour in this figure legend, the reader is referred to the web version of this article.)

composite data in Fig. 16(a), this produces a series of points on a straight line (the red line labelled PC composite using global strain). Then the maximum local (true) strain in each X-ray image is found, and this is combined with the fit to the matrix data in Fig. 16(a) to infer the local temperature rise corresponding to this maximum strain, which is a series of somewhat scattered points. If the maximum local strains observed in the ESRF X-ray data are consistent with the peak temperatures observed in the IR experiments, the points should lie around the line, which is indeed observed at low global strains. The increasing disagreement with increasing global strain may be attributed to the inability of the DIC analysis to accurately capture the strain localisation at large strains due to the use of the projection through the whole specimen or uncertainty in the thermal measurements owing to the localisation.

4.3.4. Summary of temperature rises in the rate-dependent compression experiments

Fig. 17 shows the temperature rise for the two materials at four adiabatic strain rates between 0.5 and 2500 s⁻¹. As expected, the higher strain rate experiments have higher temperature rises and a more significant difference, in the composite, between the peak and mean temperatures. High strain rates can enhance localisation behaviour, and the stiffness is reduced rapidly because of the significant temperature rise in the adiabatic shear bands. Combined with the X-ray data, the implication is that adiabatic strain localisation plays a more significant role than microcracking in softening of these materials.

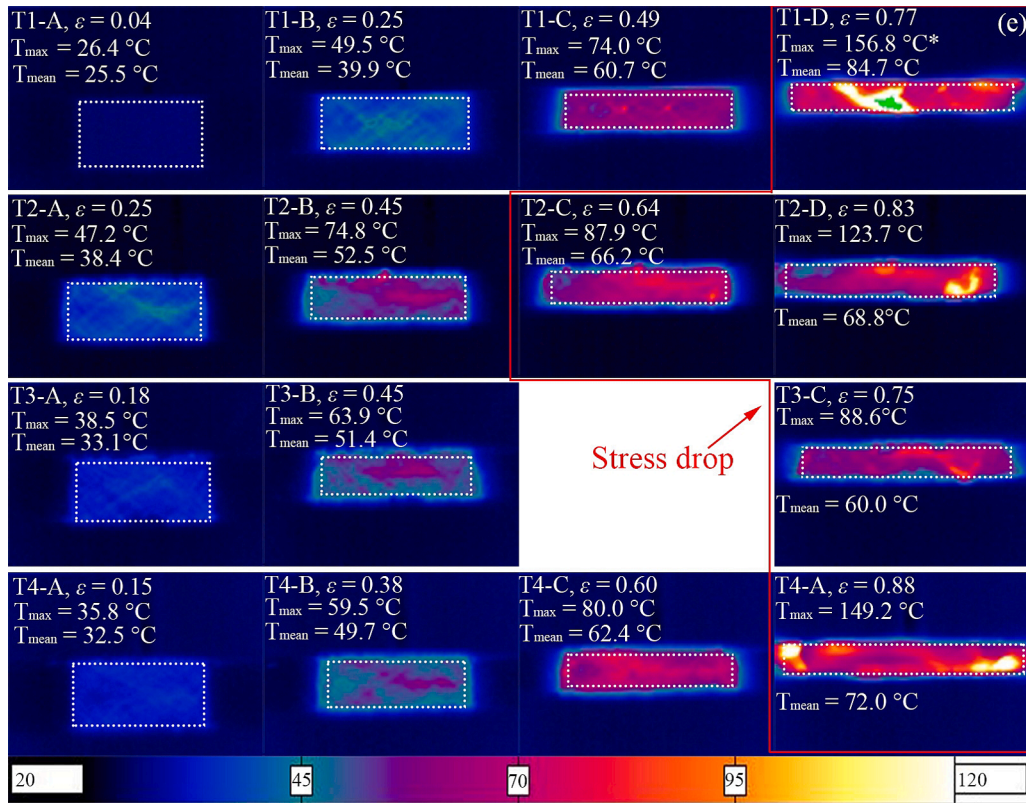


Fig. 13. (continued).

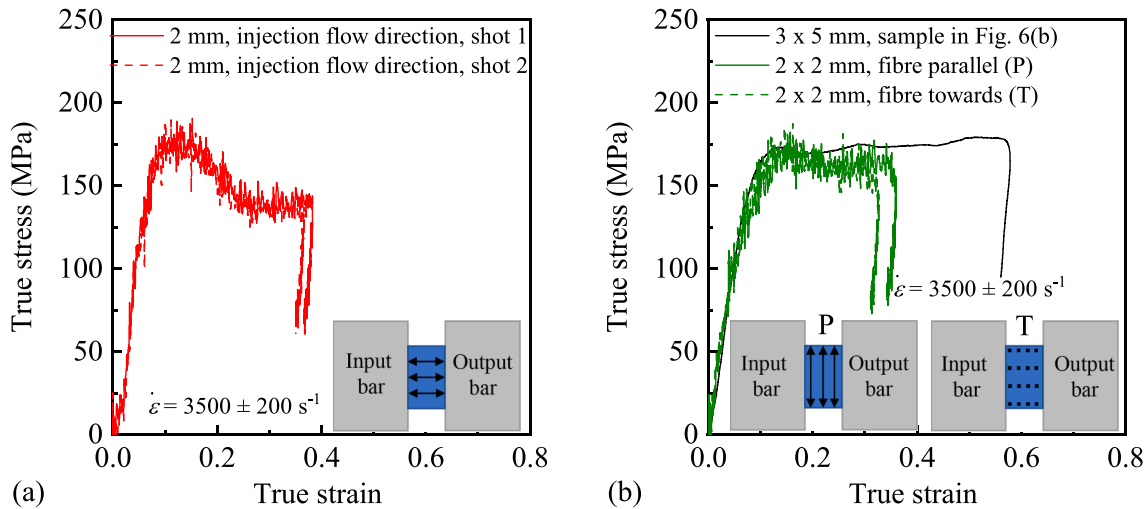


Fig. 14. True stress versus true strain curves: (a) In-plane specimens (2 × 2 mm), loaded in the injection flow direction (b) Through thickness specimens (2 × 2 mm) with the injection flow direction parallel (P) and perpendicular (T) to the image plane.

5. Conclusions

Thermomechanical characterisation of a polycarbonate composite with 20 wt% glass fibre reinforcement has been performed alongside the matrix polycarbonate materials. Frequency sweep dynamic mechanical analysis (DMA) tests were performed on the composite material cut at 0°, 45° and 90° to the fibre flow direction, as well as the matrix and used to construct time–temperature superposition master curves. Tensile samples were obtained in different orientations and loaded at different speeds; all samples displayed rate dependent failure (composite) or yield (PC matrix) stresses. Temperature dependent compression experiments

were performed from −60 to 120 °C, and rate dependent compression experiments from 0.001 s^{−1} to above 5000 s^{−1}. The results for both materials display time–temperature equivalence: a decrease in temperature has the same effect as an increase in strain rate. The yield stress shows a bilinear increase with the increased logarithm of rate for both matrix and composite material due to the secondary (β)-transition. For large strains the equivalence is less, in particular, increased softening is observed in the high-rate experiments compared to their equivalent quasi-static low temperature tests. Two possible reasons for the softening are assumed: thermal softening and microcracking. Using an IR camera, temperature rises during deformation are measured for strain

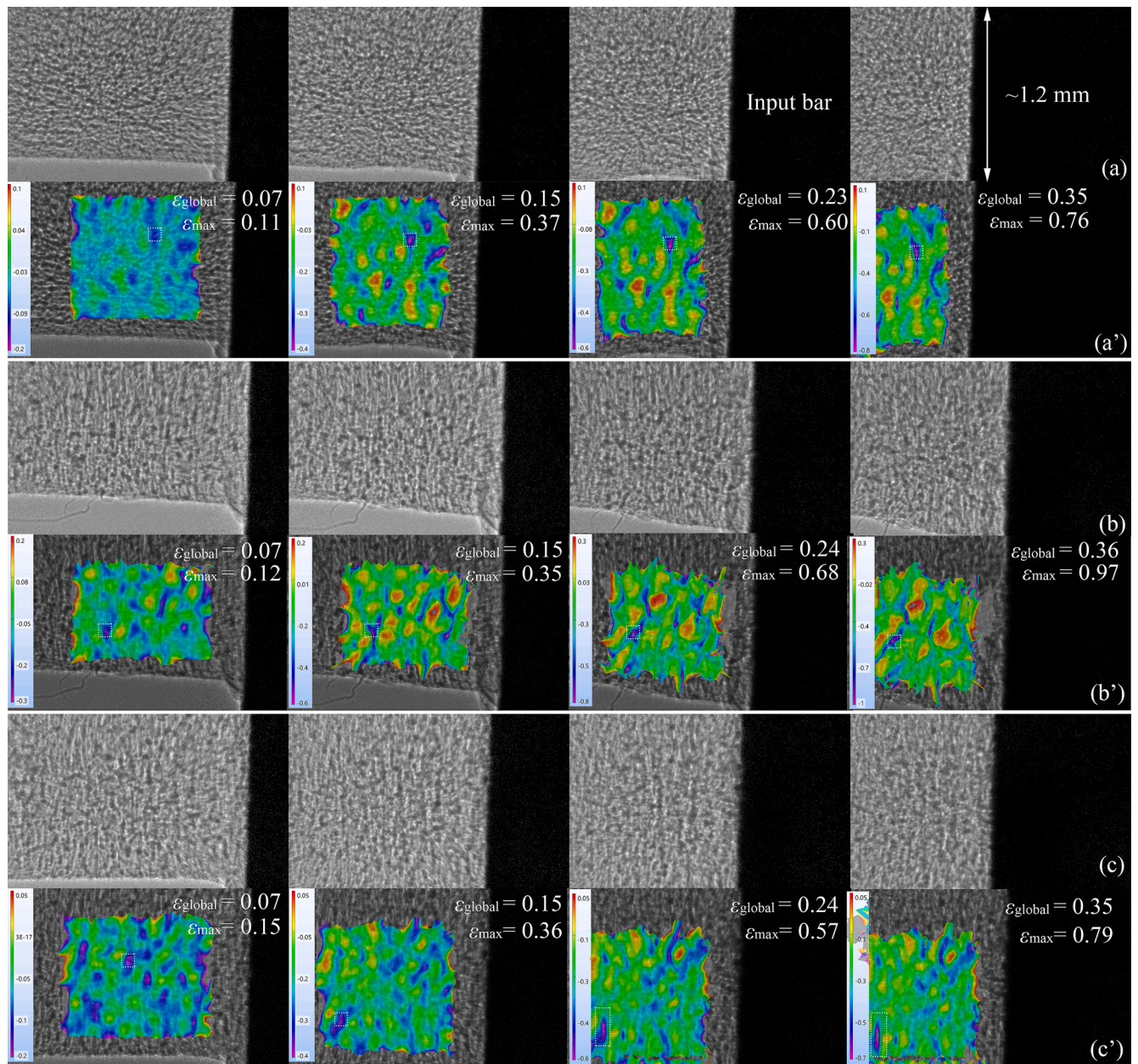


Fig. 15. X-ray images and DIC mapping for 2×2 mm samples: (a) and (a') loaded in the injection flow direction, (b) and (b') injection flow direction parallel to the image plane (P), (c) and (c') injection flow direction perpendicular to the image plane (T). Zoomable images will be made available online.

rates between 0.01 and 2500 s^{-1} . In all cases, the PC matrix deforms homogeneously, with a larger temperature rise at the higher strain rates: the maximum temperature achieved through self-heating in the LSHPB tests is about 80°C . The experiments for PC composite reveal the rate-dependent deformation process that the higher strain rate can lead to a higher rise in temperature at the same strain level. The thermal localisation is observed in high rate tests on the PC composites, with a divergence between the maximum local and mean temperature, which increases with increasing strain until it reaches around 80°C at 0.6 true strain. Here, a rapid stress drop is observed, accompanied by adiabatic shear bands in which the temperature can reach the glass transition temperature ($\sim 150^\circ\text{C}$) of the matrix material. At medium rates, some localisation is observed, but this does not lead to shear band formation. To further investigate localisation, in-situ split Hopkinson pressure bar (SHPB) tests were performed in ESRF using ultra-fast X-ray imaging, which was combined with DIC analysis to produce strain maps in the specimen. The X-ray images did not reveal failures, such as debonding

and cracks, but did show strain localisations that were consistent with the temperature rises observed in the IR images. These temperature rises were used to link global and local behaviours in the composite, which further reinforces the conclusion that softening in these materials at high strain rates is a result of adiabatic shear band formation. In the future, microscopy measurements of samples loaded in different conditions are recommended to provide more detailed internal information. Moreover, the rate- and temperature-dependent finite element model is suggested to understand the experimental observations.

CRediT authorship contribution statement

Peihao Song: Conceptualization, Data curation, Formal analysis, Investigation, Methodology, Writing – original draft. **David J. Chapman:** Investigation, Methodology, Writing – review & editing. **Aaron M. Graham:** Investigation, Writing – review & editing. **Bratislav Lukić:** Investigation, Methodology, Writing – review & editing.

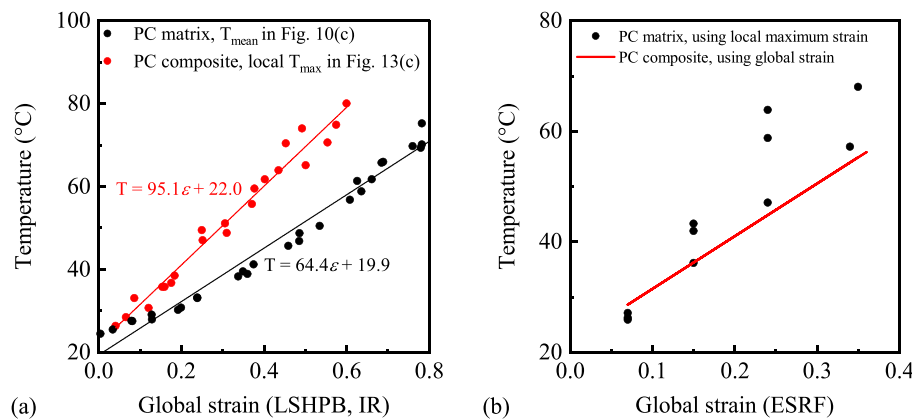


Fig. 16. (a) Temperature vs strain for PC matrix and maximum temperature vs strain for PC composite, (b) Temperature change inferred using global strain in ESRF data compared to temperature change inferred using local maximum strain in ESRF data.

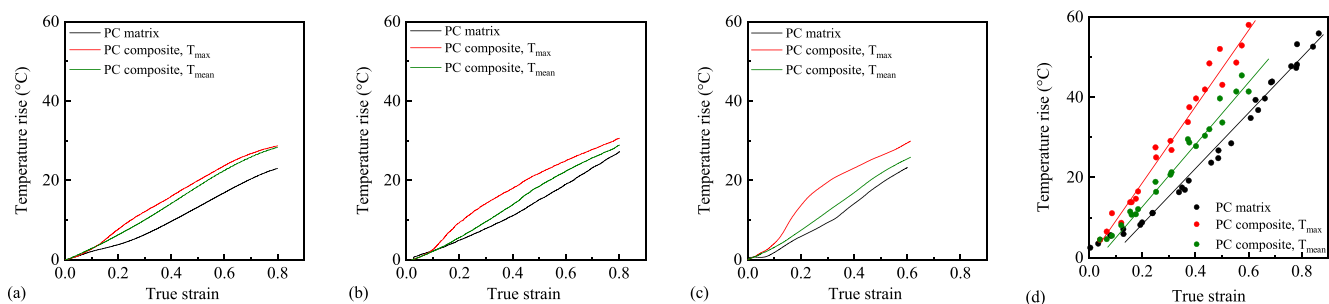


Fig. 17. Temperature rise comparison for PC and its composite at different strain rates: (a) 0.5 s^{-1} , (b) $\sim 1.5 \text{ s}^{-1}$, (c) $\sim 12 \text{ s}^{-1}$, (d) $\sim 2500 \text{ s}^{-1}$.

Alexander Rack: Investigation, Methodology. **Clive R. Siviour:** Conceptualization, Project administration, Supervision, Writing – review & edit, Funding acquisition..

Declaration of competing interest

The authors declare that they have no known competing financial interests or personal relationships that could have appeared to influence the work reported in this paper.

Data availability

Data will be made available on a repository managed by the University of Oxford at DOI: 10.5287/ora-dakrm9m4e.

Acknowledgements

This research forms part of the research programme of DPI, project

827t19, *Impact Modelling of Polymers: high-Rate Experiments for Solid-state Simulations* and the polycarbonates were kindly supported by Saudi Basic Industries Corporation (SABIC). The authors thank our colleagues on this project, Dr Davide De Focatiis and Grace Owen at the University of Nottingham for helpful discussions. We also thank the technicians of the Solid Mechanics Group workshop, in particular, Andy Bateman for his help with the manufacture of specimens and fixtures for this project and Nicholas Hawkins for his help with the DMA tests. We thank the Hypersonics Research Group for the use of the high speed thermal imaging camera, and thank EPSRC for support of thermomechanical characterisation as part of EP/V003321/1. X-ray imaging was performed at ESRF under proposal beamtime MI-1397, under the Shock BAG supported by the European Union's Horizon 2020 research and innovation program under Grant Agreement No. 870313, Streamline). For the purpose of Open Access, the authors have applied a CC BY public copyright license to any Author Accepted Manuscript (AAM) version arising from this submission.

Appendix A

Table A1

Adopted Digital Image Correlation (DIC) setup.

DIC software	MatchID, version 2023.1.1
Image filtering	Gaussian, $5 \times 5 \text{ pixel}^2$ kernel
Subset size (pixel)	21
Step size (pixel)	2
Subset shape function	Quadratic
Matching criterion	Zero-normalised sum of square differences (ZNSSD)
Interpolant	Local Bicubic Spline Interpolation
Strain tensor	Hencky (True) strain tensor
Estimates progress history	Spatial and updated reference
Strain window size	$13 \times 13 \text{ pixels}^2$, Quadratic Quadrilateral

References

- [1] Hsissou R, Seghiri R, Benzekri Z, Hilali M, Rafik M, Elharfi A. Polymer composite materials: A comprehensive review. *Compos Struct* 2021;262:113640.
- [2] Chen C, Zhang C, Zhao Z, Wang Y, Wong S-C, Li Y. Effect of fiber reinforcement and fabrication process on the dynamic compressive behavior of PEEK composites. *Int J Mech Sci* 2019;155:170–7.
- [3] Fu S-Y, Lauke B, Mai YW. Science and engineering of short fibre-reinforced polymer composites. Woodhead Publishing; 2019.
- [4] Pastukhov LV, Govaert LE. Plasticity-controlled failure of fibre-reinforced thermoplastics. *Compos B Eng* 2021;209:108635.
- [5] Bernasconi A, Cosmi F. Analysis of the dependence of the tensile behaviour of a short fibre reinforced polyamide upon fibre volume fraction, length and orientation. *Procedia Eng* 2011;10:2129–34.
- [6] Pastukhov LV, Govaert LE. Crack-growth controlled failure of short fibre reinforced thermoplastics: Influence of fibre orientation. *Int J Fatigue* 2021;143:105982.
- [7] De Monte M, Moosbrugger E, Quaresimin M. Influence of temperature and thickness on the off-axis behaviour of short glass fibre reinforced polyamide 6.6-cyclic loading. *Compos A Appl Sci Manuf* 2010;41(10):1368–79.
- [8] Engels TAP, van Breemen LCA, Govaert LE, Meijer HEH. Predicting the long-term mechanical performance of polycarbonate from thermal history during injection molding. *Macromol Mater Eng* 2009;294(12):829–38.
- [9] Janssen RPM, de Kanter D, Govaert LE, Meijer HEH. Fatigue life predictions for glassy polymers: a constitutive approach. *Macromolecules* 2008;41(7):2520–30.
- [10] Song P, Trivedi AR, Siviour CR. Mechanical response of four polycarbonates at a wide range of strain rates and temperatures. *Polym Test* 2023;107986.
- [11] Amiri-Rad A, Pastukhov LV, Govaert LE, Van Dommelen JAW. An anisotropic viscoelastic-viscoplastic model for short-fiber composites. *Mech Mater* 2019;137:103141.
- [12] Amiri-Rad A, Hütter M, Govaert LE, van Dommelen JAW. Improved associated flow rule for anisotropic viscoplasticity in thermoplastic polymer systems. *Mech Mater* 2021;163:104087.
- [13] Ozkan C, Karsli NG, Aytac A, Deniz V. Short carbon fiber reinforced polycarbonate composites: Effects of different sizing materials. *Compos B Eng* 2014;62:230–5.
- [14] Amiri-Rad A, Wismans M, Pastukhov LV, Govaert LE, van Dommelen JAW. Constitutive modeling of injection-molded short-fiber composites: characterization and model application. *J Appl Polym Sci* 2020;137(41):49248.
- [15] Ho K-C, Jeng M-C. Tribological characteristics of short glass fibre reinforced polycarbonate composites. *Wear* 1997;206(1–2):60–8.
- [16] Siviour CR, Jordan JL. High strain rate mechanics of polymers: a review. *J Dyn Behav Mater* 2016;2:15–32.
- [17] Perry JI, Walley SM. Measuring the effect of strain rate on deformation and damage in fibre-reinforced composites: a review. *J Dyn Behav Mater* 2022;8(2):178–213.
- [18] Chen WW, Song B. Split Hopkinson (Kolsky) bar: design, testing and applications. Springer Science & Business Media; 2010.
- [19] Gu J, Cao J, Qiang Y, Zhao Z, Zhang C. Rate-dependent tensile behavior and statistic strength model for fiber tow composites. *Polym Test* 2023;122:108021.
- [20] Wang H, Dong C, Hu W, Dang H, Du C, Ou Y, et al. Time-dependent high-temperature compressive failure behavior of high-silica/boron-phenolic composites modified with boron carbide and talc. *Compos Sci Technol* 2022;221:109226.
- [21] Wang H, Gong Z, Hao Y, Deng Y, Zhang C. Evolution of strain-rate dependent compressive failure behavior of ceramifiable FRP composites at high temperature conditions. *Compos Sci Technol* 2023;241:110145.
- [22] Siviour CR, Walley SM, Proud WG, Field JE. The high strain rate compressive behaviour of polycarbonate and polyvinylidene difluoride. *Polymer* 2005;46(26):12546–55.
- [23] Mulliken AD, Boyce MC. Mechanics of the rate-dependent elastic–plastic deformation of glassy polymers from low to high strain rates. *Int J Solids Struct* 2006;43(5):1331–56.
- [24] Kendall MJ, Siviour CR. Experimentally simulating high-rate behaviour: rate and temperature effects in polycarbonate and PMMA. *Philosophical Transactions of the Royal Society A: Mathematical, Physical and Engineering Sciences*. 2014;372(2015):20130202.
- [25] Trivedi AR, Song P, Siviour CR. Experimentally simulating adiabatic behaviour: capturing the high strain rate compressive response of polymers using low strain rate experiments with programmed temperature profiles. *Polym Test* 2022;116:107773.
- [26] Zhang L, Townsend D, Petrinic N, Pellegrino A. Temperature dependent dynamic compressive response of PA66-GF30 composite under constant strain rate multiaxial loading. *Compos B Eng* 2022;234:109738.
- [27] Pournoori N, Soares GC, Orell O, Palola S, Hokka M, Kanerva M. Adiabatic heating and damage onset in a pultruded glass fiber reinforced composite under compressive loading at different strain rates. *Int J Impact Eng* 2021;147:103728.
- [28] Tang Z, Chen C, Li A, Deng Y, Zhang C, Li Y. Temperature- and strain-rate-dependent tensile failure behavior of short-fiber-reinforced PEEK composites. *Compos B Eng* 2023;250:110455.
- [29] Li Z, Lambros J. Strain rate effects on the thermomechanical behavior of polymers. *Int J Solids Struct* 2001;38(20):3549–62.
- [30] Kendall MJ, Siviour CR. Experimentally simulating adiabatic conditions: approximating high rate polymer behavior using low rate experiments with temperature profiles. *Polymer* 2013;54(18):5058–63.
- [31] Pournoori N, Corrêa Soares G, Lukić B, Isakov M, Belone MCL, Hokka M, et al. In situ damage characterization of CFRP under compression using high-speed optical, infrared and synchrotron X-ray phase-contrast imaging. *Compos A Appl Sci Manuf* 2023;175:107766.
- [32] Arruda EM, Boyce MC, Jayachandran R. Effects of strain rate, temperature and thermomechanical coupling on the finite strain deformation of glassy polymers. *Mech Mater* 1995;19(2–3):193–212.
- [33] Regev A, Rittel D. Simultaneous transient temperature sensing of impacted polymers using infrared detectors and thermocouples. *Exp Mech* 2008;48:675–82.
- [34] Goviazin GG, Shirizly A, Rittel D. A Comparative study of the performance of IR detectors vs. high-speed cameras under dynamic loading conditions. *Exp Mech* 2022:1–10.
- [35] Bjerke T, Li Z, Lambros J. Role of plasticity in heat generation during high rate deformation and fracture of polycarbonate. *Int J Plast* 2002;18(4):549–67.
- [36] Lerch V, Gary G, Hervé P. Thermomechanical properties of polycarbonate under dynamic loading. *J Phys IV France* 2003;110:159–64.
- [37] Garg M, Mulliken AD, Boyce MC. Temperature rise in polymeric materials during high rate deformation. *J Appl Mech* 2008;75(1).
- [38] Lin P, Cheng S, Wang S-Q. Strain hardening during uniaxial compression of polymer glasses. *ACS Macro Lett* 2014;3(8):784–7.
- [39] Rittel D. On the conversion of plastic work to heat during high strain rate deformation of glassy polymers. *Mech Mater* 1999;31(2):131–9.
- [40] Tarfaoui M, El Moumen A, Yahia HB. Damage detection versus heat dissipation in E-glass/Epoxy laminated composites under dynamic compression at high strain rate. *Compos Struct* 2018;186:50–61.
- [41] Deng S, Hou M, Ye L. Temperature-dependent elastic moduli of epoxies measured by DMA and their correlations to mechanical testing data. *Polym Test* 2007;26(6):803–13.
- [42] Gray III GT, Blumenthal WR. Split-Hopkinson pressure bar testing of soft materials. *ASM handbook* 2000;8:488–96.
- [43] Chen WW, Song B. Dynamic characterization of soft materials. *Dynamic Failure of. Mater Struct* 2010:1–28.
- [44] van der Tempel L. Thermography of semi-transparent materials by a FLIR ThermoCAM SC3000 infrared camera. Philips Research. 2011.
- [45] Weitkamp T, Tafforeau P, Boller E, Cloetens P, Valade JP, Bernard P, et al. Status and evolution of the ESRF beamline ID19. 1 ed: American Institute of Physics. p. 33–8.
- [46] Cohen A, Levi-Hevroni D, Fridman P, Chapman D, Rack A, Olbinado MP, et al. In-situ radiography of a split-Hopkinson bar dynamically loaded materials. *J Instrum* 2019;14(06):T06008.
- [47] Escauriza EM, Olbinado MP, Rutherford ME, Chapman DJ, Jonsson JCZ, Rack A, et al. Ultra-high-speed indirect x-ray imaging system with versatile spatiotemporal sampling capabilities. *Appl Opt* 2018;57(18):5004–10.
- [48] Lukić B, Saletti D, Forquin P, Blasone M, Cohen A, Rack A. Single bunch X-ray phase-contrast imaging of dynamic tensile failure in geomaterials. *J Dyn Behav Mater* 2022:1–13.
- [49] Plass CT, Bonino V, Ritzler M, Jäger LR, Rey-Bakakioa V, Hafermann M, et al. Spatially resolved dynamics of cobalt color centers in ZnO nanowires. *Adv Sci* 2023;10(1):2205304.
- [50] Wilkins SW, Gureyev TE, Gao D, Pogany A, Stevenson AW. Phase-contrast imaging using polychromatic hard X-rays. *Nature* 1996;384(6607):335–8.
- [51] Palmese GR, McCullough RL, Sottos NR. Relationship between interphase composition, material properties, and residual thermal stresses in composite materials. *J Adhes* 1995;52(1–4):101–13.
- [52] Sottos NR, McCullough RL, Scott WR. The influence of interphase regions on local thermal displacements in composites. *Compos Sci Technol* 1992;44(4):319–32.
- [53] Skourlis TP, McCullough RL. The effect of temperature on the behavior of the interphase in polymeric composites. *Compos Sci Technol* 1993;49(4):363–8.
- [54] SABIC. LEXAN™ FR RESINS 3412R Data Sheet. 2023.